Final Technical Report for DOE EERE Project DE-EE0006925
(01/01/2015 ~ 12/31/2017)

"Hybrid Ionic-Nano-Additives for Engine Lubrication to Improve Fuel Efficiency"

Project Team:

University of Tennessee Knoxville (UTK): Bin Zhao and Sheng Dai
Oak Ridge National Lab (ORNL): Jun Qu, Huimin Luo and Beth Armstrong
University of California Merced (UCM): Ashlie Martini

Reported by PI: Bin Zhao
Department of Chemistry
University of Tennessee
Knoxville, TN 37996
Phone: 865-974-3399
Email: bzhao@utk.edu

March 31, 2018

Summary: We developed a new class of hybrid organic-inorganic/metallic nanoparticles (NPs) as additives for polyalphaolefin (PAO) for friction and wear reduction to improve engine energy efficiency. The hybrid additives were synthesized by using polymers, ionic liquid (IL)-containing polymers, organic ligands, or ILs to functionalize NPs. The tribological properties of these hybrid NPs or mixtures of NPs and ILs were studied by high contact stress ball-on-flat reciprocating sliding tests at 100 °C. Significant reductions in friction and wear were achieved compared to PAO base oil. The lubrication mechanisms were elucidated by both experimental and simulation studies.

Technical Accomplishments:

- Oil-soluble polymer brush-grafted metal oxide nanoparticles (hairy NPs) were synthesized by surface-initiated "living"/controlled radical polymerization. These hairy NPs exhibited excellent dispersibility and stability in polyalphaolefin (PAO) over a wide temperature range and demonstrated significant reductions in both friction and wear in high contact-stress ball-on-flat tribological tests comparted to PAO base oil.
- The effects of chemical composition of polymer brushes on oil dispersibility, stability and lubricating performance of hairy NPs were investigated, and the gained understanding provides a guideline for the design of hairy NPs as additives for friction and wear reduction.
- Improved lubricating performance was observed when hairy silica NPs and an IL were combined as an additive for PAO, and the mechanism was revealed.
- Several type of organic-modified metallic NPs, including Ag, Pd, and synergistic Ag-NP pair, were synthesized and demonstrated great potential as lubricant additives for friction and wear reduction.
- Simulation study revealed the effect of surface roughness and NP size on lubricating performance of NPs.

1. Polymer Brush-Grafted Nanoparticles (Hairy NPs) as Lubricant Additives for Friction and Wear Reduction

1.1. Hairy Silica and Titania NPs as PAO Additives for Friction and Wear Reduction

NPs are a class of promising oil additives for friction and wear reduction because of their potential desired interactions with metal substrates and readily tunable size, chemical composition, and surface functional groups. Previous studies have shown that with the addition of NPs of metals, metal oxides, or metal sulfides, the oil lubricating performance is improved due to the function of NPs in the interfacial rubbing zone and the formation of protective tribofilms on the surface of substrates. However, a major issue with the use of NPs is their tendency to undergo aggregation and precipitation in nonpolar oils, for example, synthetic base oil PAO. To address this problem, we have synthesized oil-soluble polymer brush-grafted metal oxide NPs by first immobilizing an initiator or a chain transfer agent onto the surface of NPs and then growing polymer chains directly from the NPs, as illustrated in Scheme 1.

Hairy NPs exhibit superior dispersibility and stability in good solvents because of the favorable enthalpic interactions between polymer brushes and solvents and the entropic steric repulsions among hairy NPs. To explore the potential application of hairy NPs as oil additives, we first synthesized poly(lauryl methacrylate) (PLMA) brushes from initiator-functionalized, 23.8 nm silica NPs (Scheme 1) by surface-initiated atom transfer radical polymerization (SI-ATRP). The initiator silica NPs were prepared by immobilizing a monochlorosilane-terminated ATRP initiator onto the surface of silica NPs. To better control the SI-ATRP and facilitate the characterization of

the grafted chains, we added a free initiator, ethyl 2-bromoisobutyrate (EBiB), into the polymerization mixtures. A series of PLMA hairy silica NPs with different molecular weights were synthesized and characterized by thermogravimetric analysis (TGA) and transmission electron microscopy (TEM). TGA showed that the weight retention of hairy NPs at 800 °C decreased with increasing brush chain length, and from TEM, the interparticle distance decreased with decreasing polymer molecular weight (Figure 1). The grafting densities of polymer brushes in these hairy NPs were found to be in the range of 0.67 to 0.73 chains/nm^2, which were calculated by using the core silica NP size, the degree of polymerization (DP) of polymer brushes, and the TGA data for initiator-functionalized NPs and hairy NPs.

Scheme 1. Synthesis of Oil-Soluble Hairy Nanoparticles by Surface-Initiated Atom Transfer Radical Polymerization (SI-ATRP) or Reversible Addition-Fragmentation Chain Transfer (SI-RAFT) Polymerization

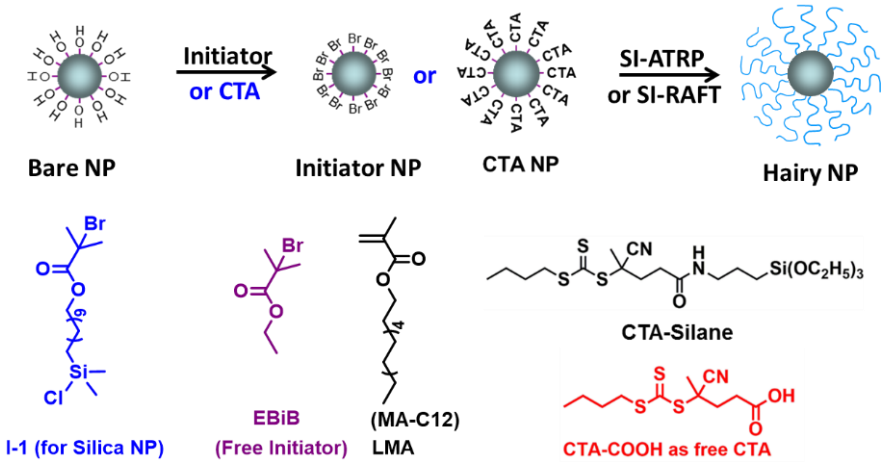

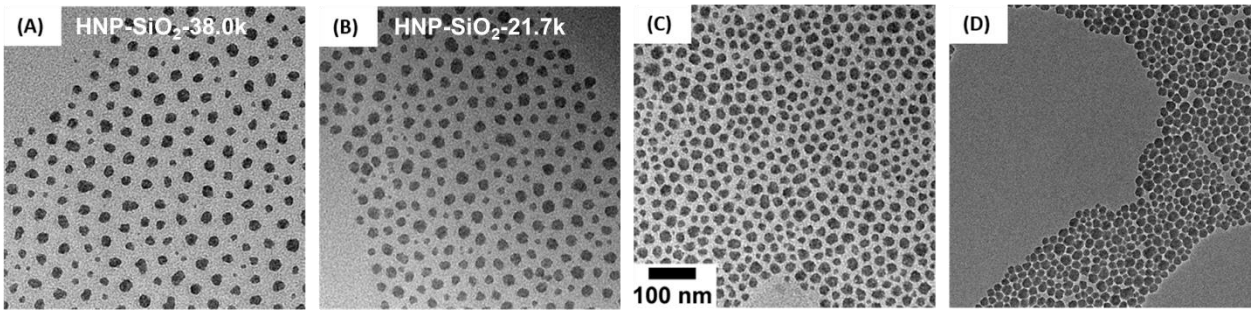

Figure 1. Bright-field TEM images of poly(lauryl methacrylate) (PLMA) brush-grafted silica NPs with $M_{n,SEC}$ of (A) 38.0 kDa (HNP-SiO_2-38.0k), (B) 21.7 kDa (HNP-SiO_2-21.7k), (C) 11.8 kDa (HNP-SiO_2-11.8k), and (D) 4.1 kDa (HNP-SiO_2-4.1k). The scale bars are the same. The hairy NPs were cast onto carbon-coated, copper TEM grids from dispersions in $CHCl_3$ with a concentration of 4 mg/mL.

All of hairy silica NP samples can be readily dispersed in PAO Spectrasyn^{TM} 4 (ExxonMobil), forming completely transparent dispersions. To examine the stability of hairy silica NPs in PAO, three 1wt% PAO dispersions of HNP-SiO_2-4.1k were kept at -20, 22, and 100 °C, respectively. The dispersions stayed clear and no change in transparency was observed after 55 days (Figure 2A and B), demonstrating the excellent stability of these hairy NPs in PAO.

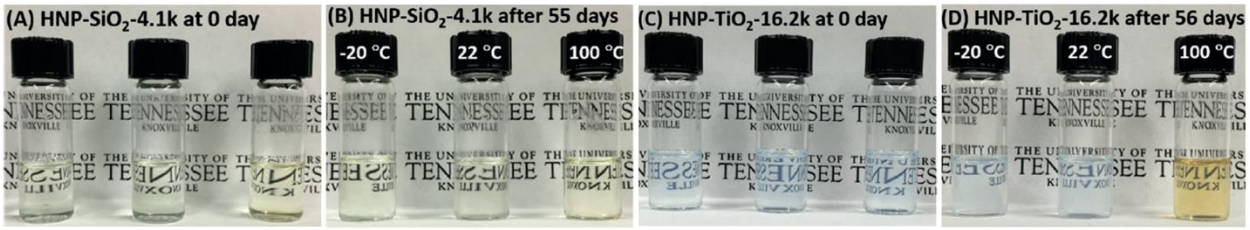

Figure 2. Photos of 1 wt% dispersions of HNP-SiO_2-4.1k in PAO in the initial state (A) and after being kept at -20, 22, 100 °C for 55 days (B), and 1 wt% dispersions of HNP-TiO_2-16.2k in PAO in the initial state (C) and after being kept at -20, 22, and 100 °C for 56 days.

The lubricating properties of 1 wt% dispersions of four hairy silica NP samples shown in Figure 1 in PAO were evaluated using a tribometer in a ball-on-flat reciprocating configuration at 100 °C under a normal load of 100 N. The oscillation frequency was 10 Hz with 10 mm stroke, and the sliding distance was 1000 m. Two repeat tests were carried out for each lubricant and averaged. As can be seen from Figure 3, the addition of 1 wt% of hairy NPs into the PAO let to significantly improved lubricating performance. For HNP-SiO_2-38.0k and -21.7k, the coefficient of friction (COF) was much lower than that of neat PAO over the entire sliding experiment. The use of lower molecular weight samples, HNP-SiO_2-11.8k and -4.1k, showed a noticeable improvement in COF even over the higher molecular weight samples. HNP-SiO2-4.1k performed slightly better in the beginning and at the end of the testing with the COF at 1000 m being reduced by about 30% compared with neat PAO. Overall, there appears to be a general trend that with decreasing brush molecular weight, the friction reduction increases. In addition, all of the samples showed a marked decrease in wear volume, by 85 – 93%, compared to the PAO.

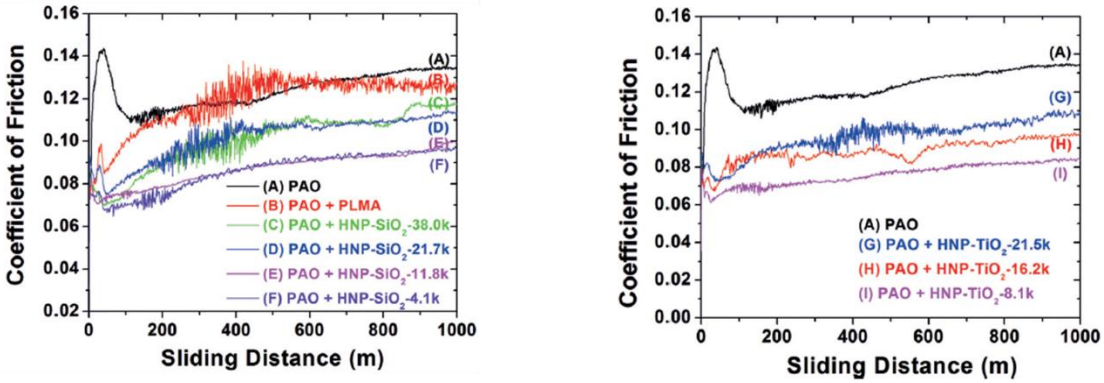

Figure 3. Friction curves for PAO SpectraSyn^{TM} 4 (A), PAO containing 1 wt% of free PLMA with a $M_{n,SEC}$ of 38.0 kDa (B), HNP-SiO_2-38.0k (C), HNP-SiO_2-21.7k (D), HNP-SiO_2-11.8k (E), HNP-SiO_2-4.1k (F), HNP-TiO_2-21.5k (G), HNP-TiO_2-16.2k (H), and HNP-TiO_2-8.1k (I). The tribological tests were performed using a Plint TE-77 tribo-tester at 100 °C under a normal load of 100 N for a sliding distance of 1000 m.

We further prepared PLMA brush-grafted TiO_2 NPs by SI-ATRP and studied their tribological properties. Anatase TiO_2 NPs with a nominal size of 15 nm were functionalized with a triethoxysilane-terminated ATRP initiator. Three PLMA brush-grafted TiO_2 NP samples with $M_{n,SEC}$ values of 21.5 kDa (HNP-TiO_2-21.5k), 16.2 kDa (HNP-TiO_2-16.2k), and 8.1 kDa (HNP-TiO_2-8.1k) were made by SI-ATRP. Like hairy silica NPs, hairy TiO_2 NPs can be well dispersed in PAO and form stable dispersions. Three 1 wt% dispersions HNP-TiO_2-16.2k in PAO were made

and kept at - 20, 22, and 100 °C, respectively. After 56 days, there were no changes in transparency observed, except the appearance of a slightly yellow color for the dispersion held at 100 °C (Figure 2C and D), presumably due to the oxidation of the residual catalyst complex in the hairy titania NPs. The tribological performances of 1 wt% hairy TiO_2 NPs in PAO were investigated. All of the hairy TiO_2-containing PAO lubricants exhibited lower COFs in the entire sliding processes compared with neat PAO, and there was a clear trend that the COF decreased with decreasing brush molecular weight (Figure 3G–I). A ~ 40% reduction in COF was observed for the lowest molecular weight sample. The wear was also reduced significantly; more than 90% reductions in wear volumes of iron flats were observed for the two lower molecular weight hairy TiO_2 samples. HNP-TiO_2-8.1k performed better than the commercially used ZDDP and amine-phosphate antiwear agents.

The friction and wear reductions with the addition of NPs resulted from the function of NPs at the interfacial zone between the two rubbing surfaces and the formation of tribofilms. To study the tribofilm, the focused ion beam (FIB) technique was used to cut a small, thin cross-section from the wear scar on the iron flat tested with 1 wt% HNP-SiO_2-4.1k, and TEM was employed to examine the area near the surface zone. As shown in Figure 4, a 200–400 nm thick tribofilm can be clearly seen, and it is an amorphous matrix embedded with small nanocrystals. Energy-dispersive X-ray spectroscopy (EDS) analysis showed that the tribofilm contained high contents of Si, Fe, and O. We believe that under the high pressure and high temperature during the tribological testing conditions, complex tribo-chemical reactions, which involved hairy NPs, occurred, producing a tribofilm on the wear track. Such a tribofilm provided a protective boundary for the underneath material and thus prevented scuffing and reduced friction and wear.

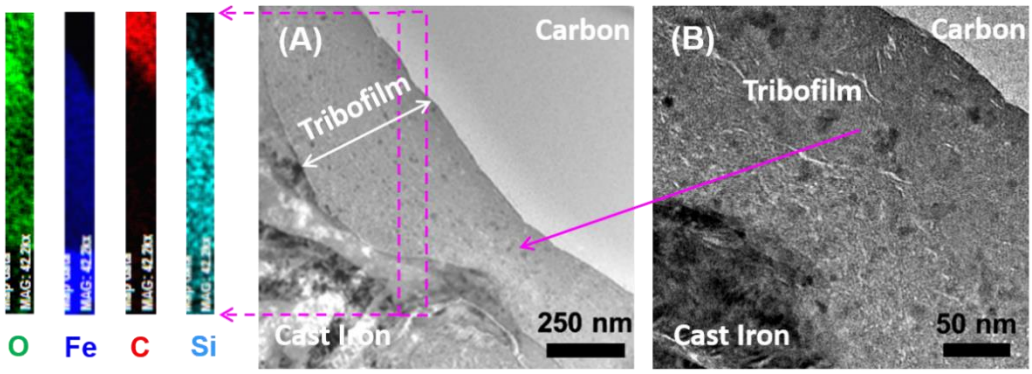

Figure 4. (A) Transmission electron microscopy (TEM) micrograph of the cross-section of the wear scar on the cast iron flat tested with 1 wt% HNP-SiO_2-4.1k-additized PAO. The element mapping data of Si, C, Fe, and O of the selected area are shown on the left. (B) Higher magnification TEM image of the area of the tribofilm pointed to by the arrow.

1.2. Effects of Alkyl Pendant Group of Polymer Brushes Grafted on Silica NPs on Oil Dispersibility, Stability, and Lubrication Property

We then studied the effects of the alkyl pendant group of poly(alkyl methacrylate) brushes on dispersibility, stability, and lubrication performance of hairy silica NPs. Surface-initiated reversible addition-fragmentation chain transfer (SI-RAFT) polymerization was employed to grow poly(alkyl methacrylate) brushes from chain transfer agent (CTA)-functionalized, 23 nm silica NPs (Scheme 1) in the presence of a free CTA. Six methacrylate monomers with various alkyl

pendant groups, *n*-hexyl methacrylate (MA-C6), 2-ethylhexyl methacrylate (MA-C8), lauryl methacrylate (MA-C12), tridecyl methacrylate (MA-C13), hexadecyl methacrylate (MA-C16), and stearyl methacrylate (MA-C18), were selected in this work for a systematic study of the effects of alkyl pendant length on the dispersibility and stability of poly(alkyl methacrylate) brush-grafted NPs in PAO and the tribological property of hairy NPs as lubricant additives for friction and wear reduction.

A total of 7 hairy silica NP samples with comparable DPs (~ 30, varying from 25 to 42) were synthesized by SI-RAFT polymerization, one sample each of MA-C6, -C8, -C12, -C16, and C18 and two samples from MA-C13. In addition, one higher molecular weight poly(MA-C8) (PC8) brush-grafted silica NP sample was prepared in order to study the effect of molecular weight on stability of PC8-NPs in PAO base oil. These samples were characterized by TGA and scanning transmission electron microscopy (STEM) (Figure 5); the molecular weights and polydispersities of corresponding free polymers formed from the added free CTA were measured by size exclusion chromatography using polystyrene standards as references. From the degrees of polymerization, core silica NP size, and the TGA, the grafting densities of polymer brushes were calculated. These data are summarized in Table 1.

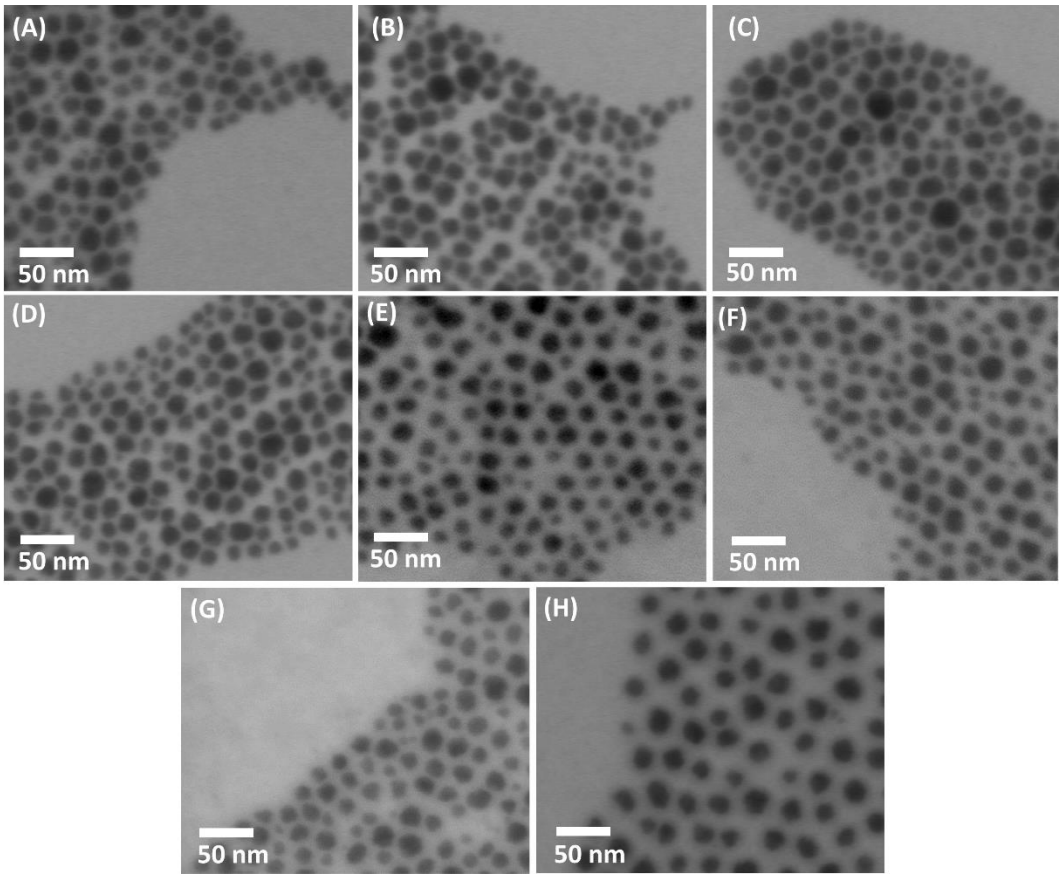

Figure 5. Bright field scanning transmission electron microscopy (STEM) micrographs of (A) PC6-NP1-7.0k, (B) PC8-NP1-7.8k, (C) PC12-NP1-9.5k, (D) PC13-NP1-9.7k, (E) PC13-NP3-7.2k, (F) PC16-NP2-8.3k, (G) PC18-NP1-13.9k, and (H) PC8-NP2-18.0k cast onto carbon-coated, copper TEM grids from 2 mg/mL dispersions of hairy silica NPs in THF.

Table 1. Characterization Data for Hairy Silica NPs and Corresponding Free Polymers

Hairy NPs	CTA-NPs [a]	Monomer [a]	$M_{n,SEC}$ [b] (kDa)	PDI [b]	DP [c]	σ [d] (chains/nm^2)
PC6-NP1-7.0k	CTA-NPs-B1	MA-C6	7.0	1.25	32	0.72
PC8-NP1-7.8k	CTA-NPs-B1	MA-C8	7.8	1.23	38	0.57
PC12-NP1-9.5k	CTA-NPs-B1	MA-C12	9.5	1.24	29	0.52
PC13-NP1-9.7k	CTA-NPs-B1	MA-C13	9.7	1.20	32	0.62
PC13-NP3-7.2k	CTA-NPs-B3	MA-C13	7.2	1.16	25	0.69
PC16-NP2-8.3k	CTA-NPs-B2	MA-C16	8.3	1.14	27	0.28
PC18-NP1-13.9k	CTA-NPs-B1	MA-C18	13.9	1.22	42	0.31
PC8-NP2-18.0k	CTA-NPs-B2	MA-C8	18.0	1.13	113	0.44

[a] The batch of CTA-NPs used for the preparation of respective hairy NP sample. [b] Number average molecular weight ($M_{n,SEC}$) and polydispersity index (PDI) of the corresponding free polymer were determined by size exclusion chromatography (SEC) relative to polystyrene standards using THF as solvent. [c] Degree of polymerization (DP) was calculated from the monomer conversion and the molar ratio of monomer to the sum of free CTA and surface-grafted CTA. [d] Grafting density (σ) was calculated using the size of silica NPs (23 nm), DP, and TGA data.

To study the dispersibility and stability of the obtained hairy silica NPs in PAO base oil, 1.0 wt% dispersions in PAO were prepared. All hairy NPs, except PC6- and PC8-grafted NPs, were fully dispersed in PAO at room temperature, forming homogeneous, transparent dispersions. Note that the original silica NPs were not stable in PAO and precipitation occurred. To examine the stability of hairy NPs in PAO, 1.0 wt% dispersions of PC13-NP1-9.7k in PAO were concurrently stored at -15 °C, 18 °C, and 100 °C. All three samples remained clear and homogeneous after 60 days, and no visible changes were observed (Figure 6A). Dynamic light scattering (DLS) was carried out at 23 °C to measure the size distribution of hairy NPs in these three dispersions and compare them to a freshly prepared dispersion of PC13-NP1-9.7k in PAO. The DLS samples were prepared by diluting the original dispersions with neat PAO to a concentration of 0.1 mg/mL. The intensity-weighted hydrodynamic size was 56.2 nm for the freshly prepared sample. This value was essentially unchanged for the samples stored at -15, 18, and 100 °C for 60 days, with the average size of 54.4 nm, 57.5 nm, and 58.9 nm, respectively. This confirmed the robustness of the polymer brush-grafted silica NPs and the high stability of these hairy NPs in PAO.

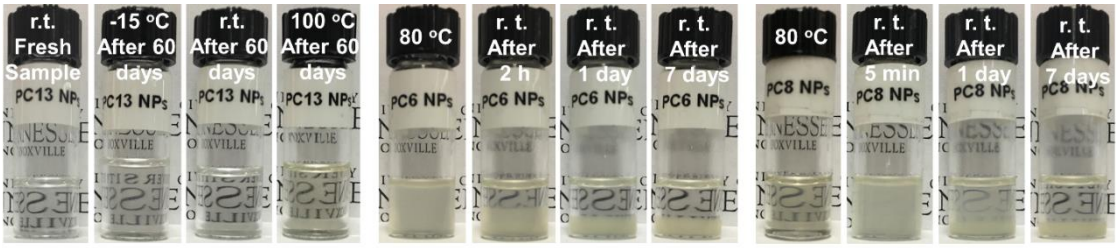

Figure 6. Optical photos of (A) a freshly prepared 1.0 wt% dispersion and three 1.0 wt% dispersions of PC13-NP1-9.7k in PAO after storage for 60 days at -15, 18, and 100 °C; (B) a 1.0 wt% dispersion of PC6-NP1-7.0k in PAO at 80 °C and sitting at r.t. for 2 h, 24 h, and 7 days after removal from a 80 °C oil bath; (C) a 1.0 wt% dispersion of PC8-NP1-7.8k in PAO at 80 °C and sitting at r.t. for 5 min, 1 day, and 7 days after removal from a 80 °C oil bath.

PC6- and PC8-grafted silica NPs cannot be dispersed in PAO to form a homogenous and clear dispersion at a concentration of 1.0 wt% at room temperature. For PC6-NP1-7.0k in PAO, heating the mixture to 80 °C resulted in no visual change, and the NPs settled out quickly upon sitting quiescently at room temperature (Figure 6B). Interestingly, the 1.0 wt% heterogeneous suspension of PC8-NP1-7.8k in PAO became clear and homogeneous upon heating at 80 °C (Figure 6C). This cloudy-to-clear transition was reversible; upon cooling at room temperature, the clear dispersion turned cloudy. The cloud point was 54 °C by visual inspection. If the brush molecular weight is increased, the cloud point would decrease, as can be seen from the cloud point (46 °C) of PC8-NP2-18.0k in PAO at a concentration of 1.0 wt%.

The tribological properties of poly(alkyl methacrylate) brush-grafted silica NPs with various alkyl pendant groups as additives for a lubricating base oil, PAO, were investigated by a ball-on-flat reciprocating configuration at 100 °C using a CL35 cast iron flat and an AISI 52100 steel ball as mentioned earlier. For all hairy NPs that readily formed homogeneous transparent dispersions in PAO at room temperature, namely PC12-, PC13-, PC16-, and PC18-grafted NPs, the COF exhibited a smooth start without scuffing and a much lower steady-state value relative to PAO throughout the sliding process (Figure 7). The friction coefficient values were between 0.08 and 0.1 at 1000 m, with PC16-NP2-8.3k exhibiting the largest friction reduction (38%) relative to the base oil. The COF traces of PC12-NP1-9.5k, PC13-NP1-9.7k, PC16-NP2-8.3k, and PC18-NP1-13.9k were all below that of PAO containing 1.0 wt% ZDDP (Figure 7A). Figure 7B shows that two PC13-grafted NP samples performed similarly; their friction curves essentially overlapped until ~ 600 m, after which PC13-NP3-7.2k exhibited slightly lower COF values. Considering the limited contribution to the friction reduction from the polymer alone (curve vii in Figure 7A), the similar tribological properties of five hairy NP samples with different alkyl groups indicated the importance of the core silica NPs in the effectiveness of hairy NPs as additives. It appears that the main function of the grafted polymer brushes is to provide colloidal stability for the silica core NPs in PAO base oil. Once a homogeneous dispersion is achieved, the number density of NPs in the lubricant is likely to be a primary factor in determining tribological performance.

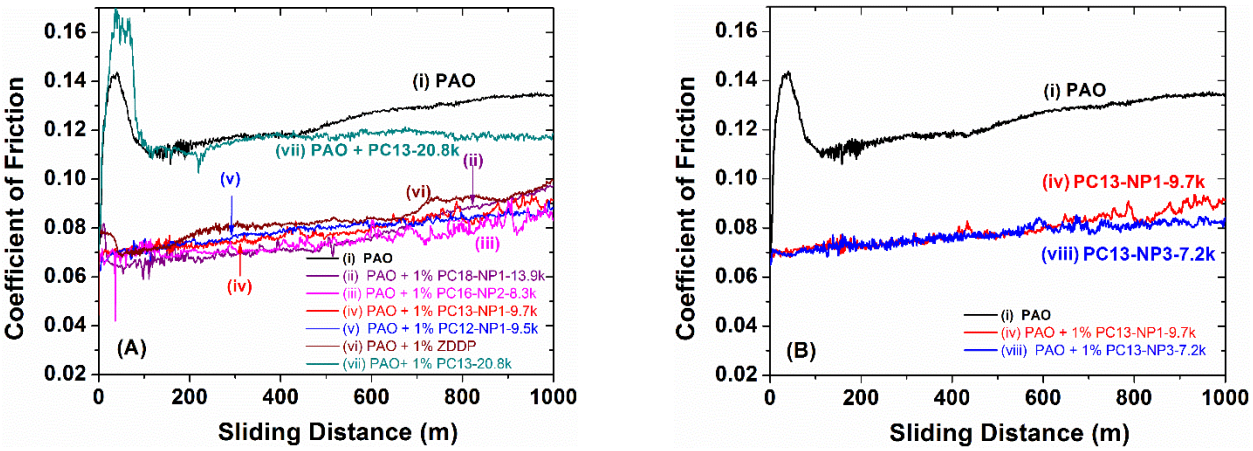

Figure 7. (A) Friction curves for PAO SpectraSyn^{TM} 4 (i), PAO containing 1.0 wt% PC18-NP1-13.9k (ii), PC16-NP2-8.3k (iii), PC13-NP1-9.7k (iv), PC12-NP1-9.5k (v), ZDDP (vi), and PC13-20.8k free polymer (vii). (B) Friction curves for PAO containing 1.0 wt% PC13-NP3-7.2k (viii) as well as neat PAO (i) and PAO + 1.0 wt% PC13-NP1-9.7k (iv) for comparison. The tribological tests were performed using a Plint TE-77 tribo-tester at 100 °C under a point contact load of 100 N for a sliding distance of 1000 m.

The wears were measured by optical surface profilometry of the scars formed on the iron flats and on the steel balls during each tribological test. The wears of the iron flats for PC18-NP1-13.9k, PC13-NP1-9.7k, PC13-NP3-7.2k, PC12-NP1-9.5k, and PC16-NP2-8.3k had similar magnitudes and ranged from 11.7 to 23 × 10^7 μm^3, which were significantly smaller (by 5 to 10 times, or reduced by 80 – 90%) than that for neat PAO (113.0 × 10^7 μm^3). However, these values were slightly higher than that for the ZDDP-containing oil (7.9 × 10^7 μm^3). The wear volumes of the steel balls for these hairy NPs, ranging from 0.019 to 0.048 × 10^7 μm^3, were reduced by > 95% compared with that for the base oil (0.786 × 10^7 μm^3), and were similar to the value for the ZDDP.

As described earlier, PC6- and PC8-grafted silica NPs could not form clear dispersions in PAO under ambient conditions. Upon heating, while the 1.0 wt% suspension of PC6-NP1-7.0k in PAO stayed cloudy, PC8-NP1-7.8k was fully dispersed in PAO forming a transparent and stable system. To characterize the tribological property of the fully dispersed PC8-NP1-7.8k, PAO with 1.0 wt% PC8-NP1-7.8k was heated to 80 °C and stirred for 30 min to achieve a clear NP dispersion. A 1.0 wt% PC6-NP1-7.0k-containing PAO was also made using the same conditions to form a visually uniform suspension. These two NP-containing lubricants were then added onto the iron flats preheated to 100 °C for tribological testing; the results are presented in Figure 8. Interestingly, PC8-NP1-7.8k performed similarly to those more easily dispersed hairy NPs (Figure 8A). The addition of 1.0 wt% PC6-NP1-7.0k into PAO, even if not dispersed, also exhibited a significant reduction in friction compared to PAO, but performed noticeably worse than those more easily dispersed hairy NPs. However, after these two samples were left to stand at ambient conditions for 7 days, the NPs settled, and the tribological benefits were lost (Figure 8).

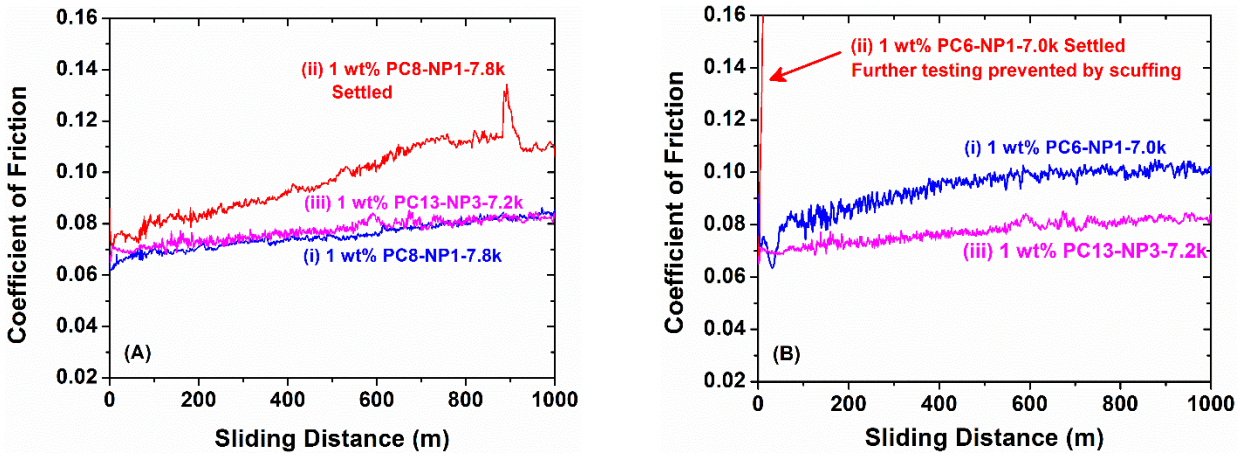

Figure 8. (A) Friction curves for PAO mixed with 1.0 wt% PC8-NP1-7.8k (i) preheated and stirred at 80 °C to achieve a full dispersion and (ii) after sitting at ambient conditions for 7 days. (B) Friction curves for PAO containing 1.0 wt% PC6-NP1-7.0k (i) preheated and stirred at 80 °C to achieve a uniform state and (ii) after sitting at room temperature for 7 days. The curve for PAO with 1.0 wt% PC13-NP3-7.2k (iii) was included for comparison. The tribological tests were performed using a tribometer at 100 °C under a load of 100 N.

1.3. Combining Oil-Soluble Hairy Silica NPs and an Ionic Liquid as an Additive for Synthetic Base Oil Polyalphaolefin (PAO)

Oil-soluble polymer-grafted metal oxide NPs and oil-miscible phosphonium-organophosphate ILs are two promising classes of lubricant additives for friction and wear reduction, with large

differences in size and chemical composition. The protective tribofilms, which contain triboactive elements from additives and are critical for wear protection and friction reduction, are formed from drastically different tribo-chemical reactions during the rubbing process. We previously observed by TEM that the typical tribofilm thickness was 10 – 400 nm for oil-miscible ILs and 200 – 400 nm for hairy silica NPs. While the anions of phosphonium-phosphate ILs can adsorb onto the metal surfaces, the hairy silica NPs exhibit little or no interaction with metals prior to the rubbing. On the other hand, phosphate anions can react with silicate to form covalent linkages, which have been utilized to improve bonding strength. If hairy silica NPs and phosphonium-phosphate ILs are used simultaneously as a lubricant additive, a further improvement in the lubricating performance might be achieved, because the phosphate anions of ILs can react with silica and metallic substrates during the tribo-chemical reactions. This could enhance the tribofilm formation and increase the bonding of the tribofilm to the substrate. To explore this possibility, we synthesized PLMA brush-grafted, 23 nm silica NPs (Scheme 1) with a brush $M_{n,SEC}$ of 6.5 kDa by SI-RAFT polymerization. The IL used in this work was tetraoctylphosphonium bis(2-ethylhexyl)phosphate ([P8888][DEHP]) whose molecular structure is shown in Scheme 2.

The stability of PLMA hairy NPs in PAO in the presence of [P8888][DEHP] was studied by dynamic light scattering. We found from DLS measurements that the size of hairy silica NPs in PAO in the presence of [P8888][DEHP] after being kept at 100 °C for 10 days was similar to that for the freshly prepared NP dispersion in PAO. Thus, PLMA hairy NPs and [P8888][DEHP] are compatible with each other when used as additives for PAO.

Scheme 2. Molecular Structure of [P8888][DEHP]

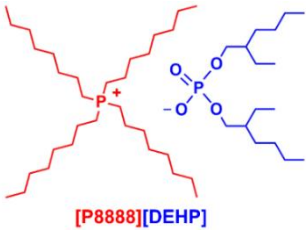

To study the effect of mixing PLMA hairy silica NPs and [P8888][DEHP] as additives, we made a set of PAO lubricant samples containing hairy NPs (HNP) and IL with an overall concentration of 2 wt% but different individual concentrations. The tribological performances of these samples were investigated by using the same high contact-stress ball-on-flat configuration at 100 °C. We found that for certain combinations the friction decreased by 20 – 35% compared with HNP or IL alone at the same concentration at the end of the sliding process. Moreover, those friction curves were significantly smoother and flatter, indicating that the combination of two different additives resulted in improved lubricating performance. To investigate the observed positive effect of combining hairy NPs and IL [P8888][DEHP] as additives for PAO, we used scanning electron microscopy coupled with energy dispersive X-ray spectroscopy (SEM-EDS) to study the tribofilms formed on the iron flats and characterize their chemical compositions. It was found that for the mixture of HNP and IL as an additive, both P and Si were enriched in the tribofilm. This indicated that both hairy NPs and IL participated in the tribo-chemical reaction to form the tribofilm for the mixture of hairy NPs and IL.

The probing depth of EDS is on the order of a few micrometers, much larger than the tribofilm thicknesses. Therefore, we further characterized the wear scars by XPS whose probing depth is 0.1 – 10 nm. As expected, the 2s and 2p peaks of both Si and P appeared for the mixture of 1% HNP + 1% IL, confirming that HNP and IL were involved in the tribo-chemical reaction to form a protective tribofilm. The core level spectra of O 1s and Si 2p showed a shift for both O 1s and Si 2p peaks, which was likely caused by the formation of new covalent linkages involving Si, O, and P from the reaction between silica core NPs and phosphate anions. By using argon-ion sputtering to etch the surface, we further obtained the composition depth profile of the tribofilm formed from the mixture of HNP + IL. The P/Si molar ratio appeared to be similar from the top surface to the interior of the tribofilm, suggesting that both HNP and IL were involved throughout the tribo-chemical reaction. Thus, both EDS and XPS suggested that the organophosphate anion of the IL reacted with silica NPs as well as the cast iron substrate surface in the tribo-chemical process, likely enhancing the tribofilm formation and strengthening the protective layer as well as its bonding with the metallic substrate. Consequently, the lubrication performance was improved as observed for the PAO lubricants containing sufficient amounts of both hairy NPs and IL.

1.4. Ionic Liquid-Incorporated Hairy Nanoparticles for Friction and Wear Reduction

As shown earlier, the main function of polymer brushes is to provide colloidal stability to core NPs. To attempt to increase the function of polymer brushes, we incorporated a polymerizable, oil-soluble phosphonium-phosphate ionic liquid into the grafted polymer chains on NPs via surface-initiated copolymerization and found that the solubility of hairy NPs in PAO decreased. Future work will focus on the design of better polymerizable ionic liquid monomers for copolymerization to make ionic liquid hairy NPs for further friction and wear reduction.

2. Organic-Modified Metal Nanoparticles as Lubricant Additives for PAO

2.1. Organic-Modified Silver Nanoparticles as Lubricant Additives

Major challenges for using metal NPs as lubricant additives include particle oxidation, agglomeration, and precipitation in oils. Surface modification may be used to convert these metal NPs into organic miscible NPs. Previous studies have shown the feasibility of using surface modification to enhance the oil solubility of metallic NPs, such as Au, Ag, Pd, Cu and Ni. Silver NPs are of our particular interest because of their chemical stability, robust synthetic protocol, and great potential in friction reduction and anti-wear properties. In this study, thiol ligands were used to modify the silver NPs due to the stable metal-thiol interface and potential for improved oil suspendability. Three types of thiol-modified Ag NPs were synthesized for studies: two 4-(tert-butyl)benzylthiol functionalized, with metallic core particle sizes of 1-3 nm and 4-5 nm (abbreviated as NP-TBBT-1 and NP-TBBT-2, respectively), and one dodecanethiol functionalized with core particle size of 3-6 nm **(**abbreviated as NP-C12). Figure 9 illustrate the model structure and morphology of the synthesized NPs. These Ag NPs are stable in both dry and liquid forms and can be stably dispersed in lubricating oils. Two tribological bench tests were carried out on the NP-containing oils: one test to investigate the friction behavior in elastohydrodynamic and mixed lubrication and the other to evaluate the friction and wear performance in boundary lubrication. The thiolated organic surface layer passivates the metallic core from oxidation, hinders the NP aggregation, and supports the solubility in hydrocarbon oils. Stable suspensions of the three samples of thiol-modified Ag NPs were achieved in a polyalphaolefin (PAO) 4 cSt base oil at various treat rates of 0.10-0.50 wt%. The NP-C12 can be directly dissolved in the PAO base oil at

a concentration up to 0.50 wt% due to the long-chain alkyl group. The TBBT-modified NPs was first dissolved in toluene (~2 wt%) as a supporting media prior to being mixed with the PAO base oil. With the help of toluene, the maximum concentrations of NP-TBBT-1 and NP-TBBT-2 that can be dissolved in PAO base oil are 0.19 and 0.38 wt%, respectively.

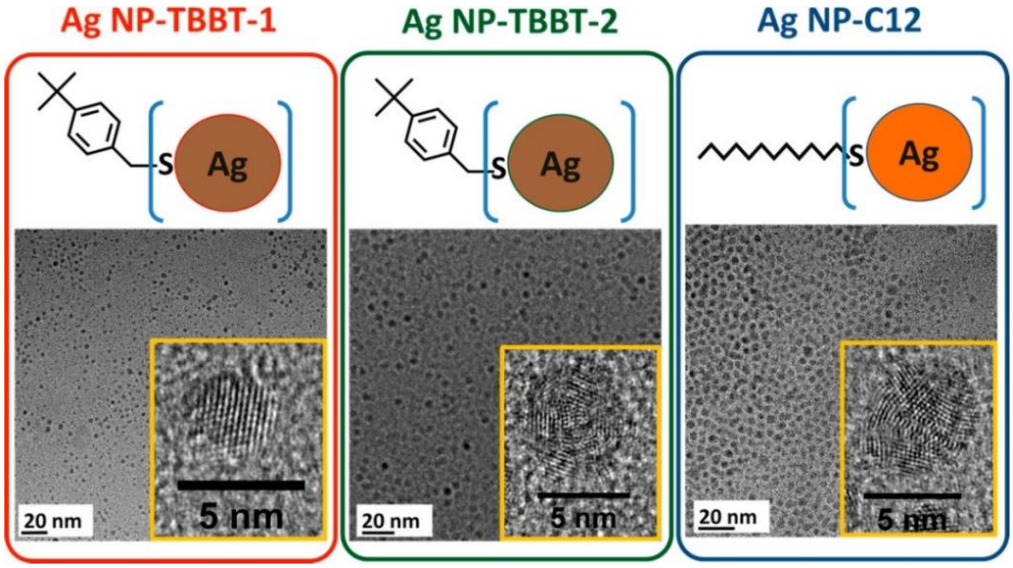

Figure 9. Model structures and morphology of thiol-modified Ag NPs. NP-TBBT-1: 4-(*tert*-butyl)benzyl thiol functionalized, core particle size of 1–3 nm; NP-TBBT-2: 4-(*tert*-butyl)benzyl thiol functionalized, core particle size of 4–5 nm; NP-C12: dodecanethiol functionalized, core particle size of 3–6 nm.

The frictional behavior of the PAO base oil and PAO+0.38 wt% NP-TBBT-2 were first investigated using a rotating cylinder sliding against a flat under a constant load of 50 N with the sliding speed decreasing from 1.2 to 0.1 m/s at a 0.1 m/s interval. The two experiment-generated Stribeck curves in the PAO base oil with and without NP-TBBT-2 are compared in Figure 10 (left). Each curve represents an average of nine replicates. Both curves showed a transition from elastohydrodynamic lubrication regime to mixed lubrication regime at around 0.5 m/s. The results show little change in friction behavior upon the addition of the Ag NPs, implying little microscopic ball-bearing effect. After testing, the contact area lubricated by the PAO+NP-TBBT-2 was examined using SEM and EDS, but no detectable Ag deposition was observed.

Figure 10 (right) shows the friction coefficient traces of all tested fluids in the boundary lubrication tests. All three thiol-modified NPs evidently reduced the friction in boundary lubrication to various extents. With the help of toluene for suspension, the oils containing the two TBBT-modified NPs (Ag core sizes of 1-3 nm and 4-5 nm, respectively) showed similar friction behavior with ~35% reduction compared to the neat base oil. The NP-C12 (3-6 nm in core size) reduced the friction coefficient by ~15% when used alone and by ~20% when toluene was added. It appeared some synergistic effect between the Ag NPs and toluene in reducing friction. Another interesting observation is that the two TBBT-NPs showed very similar friction behavior even though they have different sizes and, on the other hand, NP-TBBT-1 and NP-C12 having similar particle sizes but different organic ligands generated different friction behavior. This suggests that the friction behavior is primarily controlled by the organic ligand rather than the particle size.

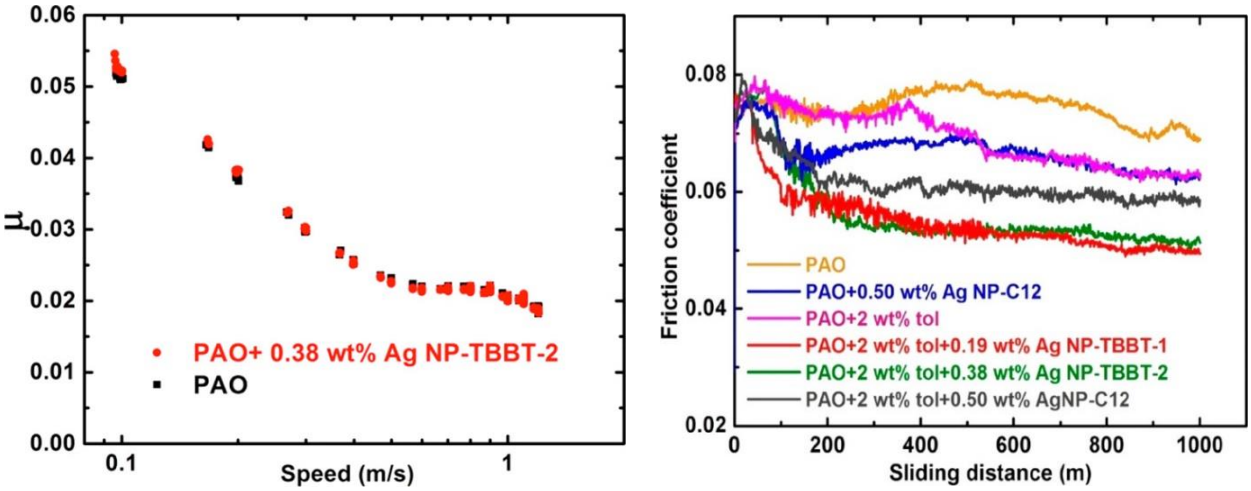

Figure 10. (Left) Stribeck curves of the neat PAO base oil (black) and PAO + NP-TBBT-2 (red). (Right) Effects of the three different Ag NPs on friction when added into the PAO base oil.

All three NPs, when added to the base oil, effectively reduced the wear volumes of both the steel ball and flat. Interestingly, the impact of toluene, NP organic ligand, and particle size on wear is very different compared with that on friction. Toluene when added into the NP-C12 oil actually increased the wear a bit, possibly due to its surface adsorption slightly hindering the tribofilm formation. The best performance was achieved by using the NP-C12 alone with the total material loss reduced by >85%. The two larger NPs, NP-C12 and NP-TBBT-2 (despite different organic ligands) are more wear protective than the smaller NP-TBBT-1. Basically opposite to the influence on the friction behavior, the particle size seemed to be more important than the organic ligand chemistry in wear protection.

In addition to the wear volume, surface roughness of the wear scars was measured along the sliding direction after each test. All the wear scars on the flats were slightly rougher than the unworn surface (10 nm), specifically, 14, 16, 31, and 20 nm (R_a) for the scars generated in the neat PAO, PAO+NP-TBBT-1, PAO+TBBT-2, and PAO+NP-C12, respectively. No clear trend of the worn surface roughness with the NP size or the type of the organic layer was observed.

For the steel flat specimen tested in the PAO oil containing NP-TBBT-2, a thin cross section was lifted out of the wear track using FIB for STEM/EDS examination. Figure 11 presents the cross-sectional STEM images and EDS elemental maps of the near surface zone, which clearly show a 50-100 nm protective tribofilm on the worn surface. Elemental mapping suggests that the matrix of the tribofilm is rich in Fe, O, and Cr, likely a mixture of FeOx and CrOx. There seem to be a number of NPs embedded in an amorphous matrix. These particles are spherical in shape with the diameter of a few nm. The Ag map overlaps very well with the particles, indicating that they are the Ag NPs from the lubricant. The Ag NPs have been confirmed to largely retain their metallic phase based on XPS analysis, suggesting their involvement was mainly through mechanical mixing rather than chemical reactions. For comparison, we conducted similar cross sectional examination of the worn steel surface lubricated by the neat PAO base oil without NPs. Unlike the NP-containing tribofilm providing a full coverage of the contact area with a relatively even thickness, the surface film without NPs appears to be thinner (<50 nm) and discontinuous. The EDS elemental mapping suggests it consisted of metal oxides.

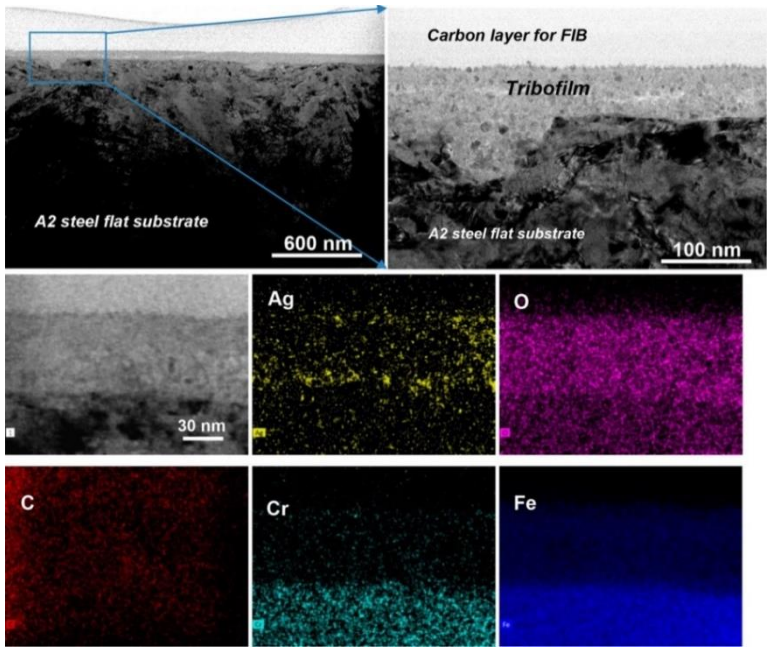

Figure 11. Bright field STEM images and EDS elemental maps of the cross section of the tribofilm formed on the steel flat lubricated by PAO + NP-TBBT-2.

In summary, organic modified Ag NPs ranging 1-6 nm in size were synthesized with different thiolated ligands as lubricant additives. The NPs' morphology and composition were examined using TEM, TGA and UV-visible spectroscopy and their tribological behavior was evaluated using steel-steel contacts in boundary as well as mixed lubrication regimes. The addition of NPs into the base oil reduced friction by up to 35% and wear by up to 85% in boundary lubrication. It is hypothesized that the molecular structure of the organic layer on the NP surface might have a bigger influence than the NP size on the friction behavior while the NP size could matter more than the organic layer in the wear protection, though NPs' lubricating performance may also be influenced by their different concentrations limited by their oil solubility. Little change in the friction behavior by Ag NPs in the mixed lubrication regime suggests insignificant mini ball-bearing rolling effect as proposed for hard NPs in the literature. Additionally, there was no evidence for surface smoothening by Ag NPs. Instead, the friction and wear reductions were attributed to the formation of a silver-rich 50-100 nm thick tribofilm as revealed by cross-sectional TEM imaging and EDS elemental mapping. Further surface chemical analysis by XPS indicated that the silver NPs largely maintained their metallic phase in the tribofilm, implying that the NPs were enclosed into the tribofilm primarily by mechanical mixing rather than chemical reactions.

2.2 Organic-Modified Pd Nanoparticles as Novel Lubricant Additives

In addition to the AgNPs, dodecanethiol modified palladium NPs were synthesized and their nanostructures and key physicochemical properties were characterized using TEM, TGA and UV-visible spectroscopy. Tribological properties of both PdNP and AgNP-containing oils were evaluated using a steel ball sliding against an iron flat at 100 ^{o}C. While both thiolated Pd and Ag NPs improved the lubrication, the Pd NPs outperformed Ag NPs in terms of oil-solubility, friction and wear reduction. The tribofilm were examined from the top surface using SEM and from the cross-section using TEM and EDS. The tribofilm composition was analyzed by XPS. It was discovered that the tribofilm formed in the lubricant containing Pd NPs was up to several

micrometer thick, which is one order magnitude thicker compared with any tribofilms reported in the literature. The thickness of a tribofilm formed by either an organic anti-wear additive, e.g., ZDDP and ionic liquid or inorganic NPs, including the Ag NPs in this study, usually is in the tens or hundreds of nanometers. No tribofilm thicker than 1 micrometer had been reported before.

Figure 12 shows the model structures, morphologies and some physicochemical properties of the synthesized Pd NP. Synthesis protocol for PdNP-C12 was similar to that of AgNP-C12, with the only difference in the metal to ligand molar ratio. TEM images of the PdNP-C12 (Figure 12 left show pseudo-spherical shapes core particles with sizes of 2-3.5 nm. This polydispersed mixture contains both crystalline and non-crystalline particle as can be seen in the high magnification images. Since these NPs are hybrid organic-inorganic materials, thermogravimetric analysis can be used to determine the temperature dependent stability and organic content. Figure 12 (right) presents the TGA curves of the Ag and Pd NPs. The decomposition temperature of the AgNP-C12 appeared to be about 50 ^{o}C higher than that of the PdNP-C12. The organic content of the AgNP-C12 and PdNP-C12 found to be 30 and 35 wt%, respectively. The TGA-determined organic content was used for designing the tribological experiments to investigate the role of the ligand. Both AgNP-C12 and PdNP-C12 can be dissolved in the PAO 4 cSt base oil up to 2 wt% in short term (several days). In longer term (several months) storage tests, the maximum stable concentrations were 0.5 wt.% and 1.0 wt.% for the AgNP-C12 and PdNP-C12, respectively.

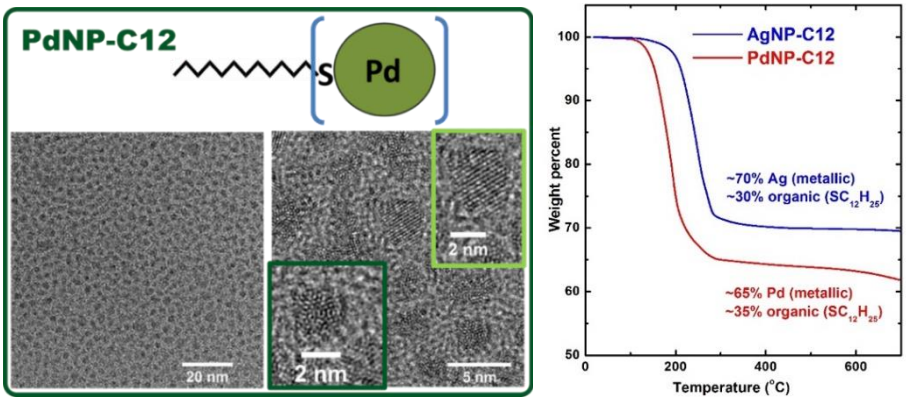

Figure 12. (Left) Model structure and morphology of PdNP-C12, core particle size of 2-3.5 nm. (Right) TGA curves of the two organic-modified NPs.

Figure 13 summarize the friction and wear results for PAO base oil and NPs-containing oils. The coefficient of friction (COF) of the neat PAO oil (black curve) had a spike (>0.17) in the first 100 m of sliding but soon dropped to and maintained around 0.13. This initial friction spike implies localized scuffing during running-in. The total wear volume of steel ball and the cast iron flat was nearly 200 $\times 10^7$ μm^3. Addition of 0.5 wt% AgNP-C12 to the PAO oil eliminated the initial friction spike (localized scuffing), decreased the steady-state COF to 0.09 (by 30%), and reduced the wear volume to 11.4 $\times$ 10^7 μm^3 (by 94%). The addition of PdNP-C12 also prevented the localized scuffing and were even more effective in friction reduction and wear protection. At the same 0.5 wt% concentration, the Pd NPs provided additional >10% reduction in the steady-state COF and additional >20% reduction in the wear volume (8.9 $\times$ 10^7 μm^3) compared with the Ag NPs.

Increasing the concentration of PdNP-C12 from 0.5% to 1.0% stabilized the friction sooner and further reduced the wear by another ~40%, as shown in Figure 13. In contrast, insignificant difference was observed for the AgNP-C12 at 0.5 and 1.0% concentrations. Overall, the PdNP-C12 convincingly outperformed the AgNP-C12.

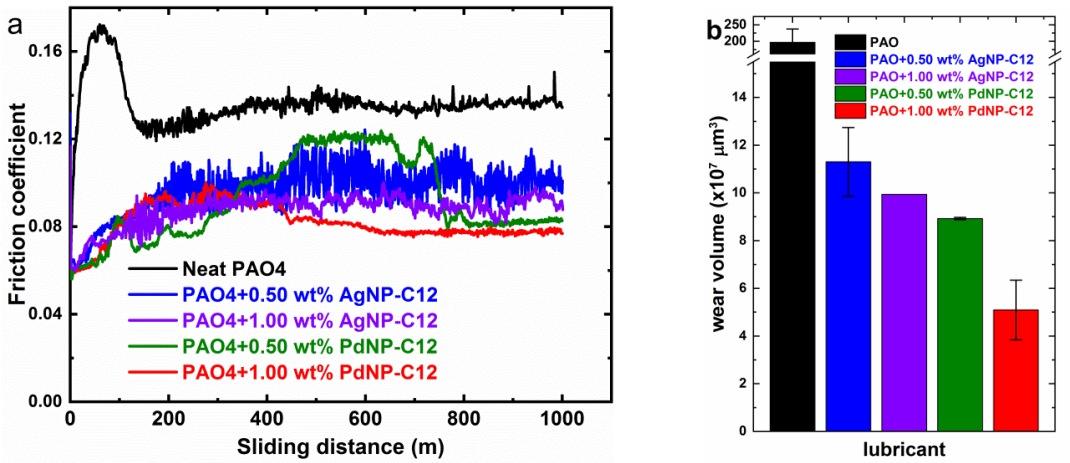

Figure 13. Comparison of (a) friction coefficient traces and (b) wear volumes produced by oils containing organic-modified Ag and Pd NPs at different concentrations. PdNP-C12 seems more effective than AgNP-C12 in reducing friction and wear.

Besides suspending the metallic NP cores in the oil, do the thiol ligands contribute to the friction and wear reductions? TGA data were used to determine the organic and inorganic contents of the AgNP-C12 and PdNP-C12. It was estimated that the PdNP-C12 and AgNP-C12 consist of ~35 wt% and ~30 wt% of the organic ligand (-$SC_{12}H_{25}$), respectively. Thus, for 1.0 wt% of PdNP-C12 in PAO, there would be 0.35 wt% of dodecanethiol. To understand the effects of the organic ligand on the lubricating behavior, 0.35 wt% dodecanethiol was dissolved into the PAO base oil and the blend was then tested in the same condition as the NPs-containing oils. Figure 14 compare the friction and wear results of neat PAO, PAO+0.35% dodecanethiol, and PAO+1.0%PdNP-C12. Addition of the dodecanethiol into the PAO reduced wear volume significantly to 15.3×10^7 µm^3, which could be attributed to the prevention of the initial localized-scuffing (no friction spike) by adsorption of the sulfur-containing ligand onto the contact surfaces. While the dodecanethiol eliminated the friction spike in running-in, it did not much affect the steady-state friction behavior (similar to that of the neat PAO). By comparing the friction and wear results of PAO+0.35% dodecanethiol and PAO+1%PdNP-C12, we can conclude that the dodecanethiol ligand possesses anti-scuffing and anti-wear functionality and is a facilitator to disperse the metallic NPs to allow them to reach the contact interface for friction reduction and additional wear protection. Similarly, there would be 0.15 wt% of dodecanethiol for 0.5 wt% of AgNP-C12 in the oil. Comparison of the PAO+0.15% dodecanethiol and PAO+0.5% AgNP-C12 showed a similar trend.

Cross-section of the worn surface near the contact zone was lifted out using FIB and prepared for STEM analysis. Figure 15 shows the cross-sectional SEM and STEM images and EDS elemental maps of the contact zone on the cast-iron flat lubricated by PAO+1.0% PdNP-C12. A surprising 2-3 µm ultra-thick tribofilm was observed (Fig. 15a), which is much thicker than the commonly reported thickness of tens to hundreds of nm for the tribofilms formed by either organic or NP-based anti-wear additives. Figure 15d depicts the cross-sectional EDS elemental maps of the selected area and the tribofilm evidently is rich with Pd and S, whose sole source is the PdNP-C12 in the oil. The tribofilm seems to contain some filaments and flakes embedded in a matrix material (appearing bright in the SEM images in Fig. 15a but dark in the STEM image in Fig. 15b.) The filaments/flakes appear to be amorphous and are likely iron oxides. Figure 15c magnifies the tribofilm matrix to reveal a nanostructure of likely aggregation of fine NPs (10-20 nm). The EDS chemical analysis shows dominant contents of Pd and S in the matrix material.

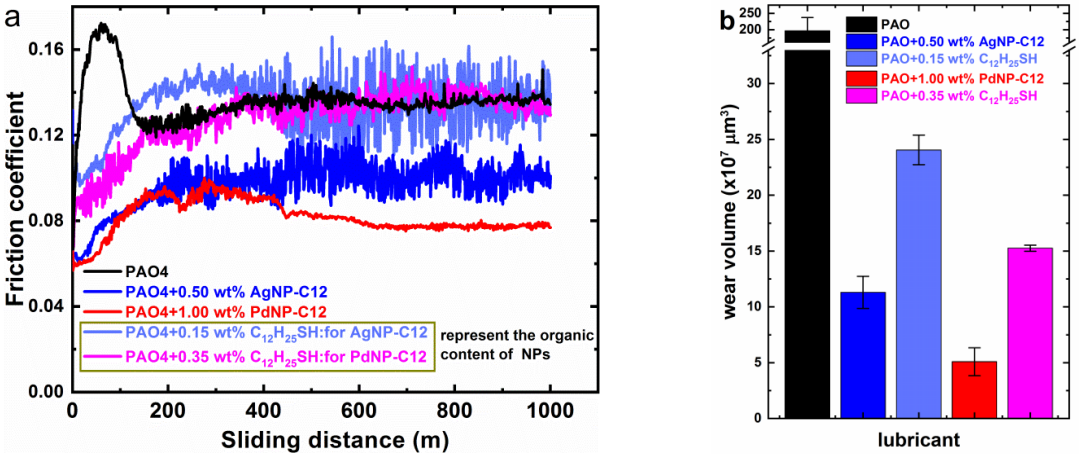

Figure 14. Comparison of (a) friction traces and (b) wear volumes produced by oils containing organic-modified NPs and the organic ligand alone. The ligand seems to possess anti-scuffing and anti-wear functionality and to be a facilitator to suspend and disperse the metallic NP cores to allow them to reach the contact interface for friction reduction and additional wear protection.

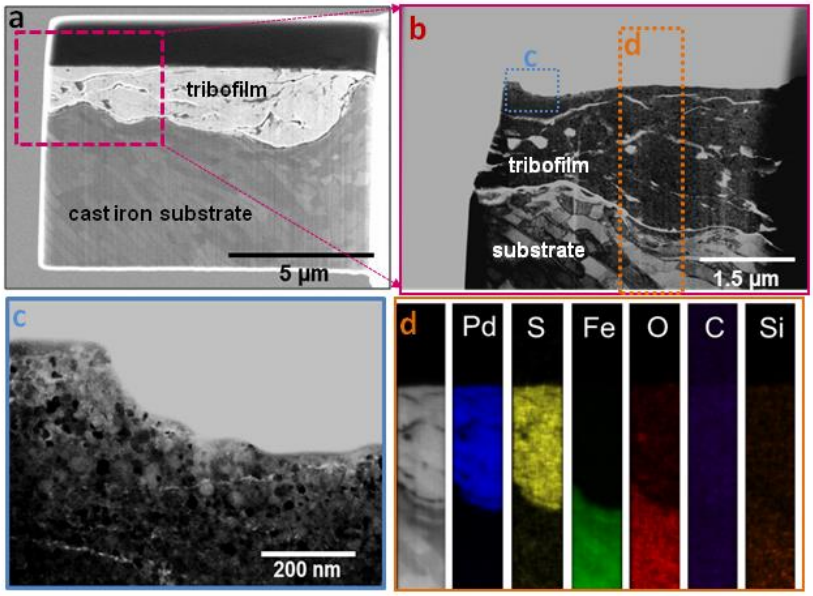

Figure 15. (a) SEM image of the FIB-lifted cross-section (before thinning) of the cast-iron flat surface lubricated with PAO+1wt% PdNP-C12. (b) Bright field STEM images of the cross-section. (c) Magnified area-blue rectangular region and (d) EDS elemental maps of the selected area.

There are several previous reports on lubrication properties of PdNP additives using tetrabutylammonium acetate and stearic acid. However, thiolated ligand shows strong affinity for the PdNP, which makes NPs more stable in ambient environment. Further, being an extreme pressure additive, thiolated ligand provides additional anti-wear performance to the metallic NPs. Metallic Pd has high catalytic activities and in combination with iron oxides can make strong-metal support interaction towards the tribochemical reaction. Further, surface adsorbed Pd NPs at contact interfaces may be converted to the Pd_4S complexes or Pd_4S nanoparticles by contact stress and frictional heating. It was reported that the temperature induced (125 ^oC) sulfur atom diffusion into the Pd nanoparticle through grain boundaries, forming sulfurized NP composition.

The sulfur atom introduced from PdNP may induced self-catalyzed C-S bond breaking at the organic layer. This C-S bond breaking and losing of organic ligand further lead to the aggregation and deposition of the PdNPs at worn surface. Therefore, the tribofilm may be a composite of Pd NPs and their complex intermediate species.

2.3. Tribological Behavior of Oil Soluble IL-Functionalized Silver Nanoparticles

Water miscible mercaptoundecanoic acid (MUA)-functionalized Ag NPs were synthesized and then modified to IL-NPs. Due to the anionic nature of the carboxylic group of the functionalized Ag NPs, several complexes were selected for modification. IL-functionalized Ag NPs showed good solubility in organic solvents, but limited solubility in the hydrocarbon base oils, up to 0.50 wt%. Figure 16 shows the friction coefficient traces of the neat PAO 4 cSt base oil and the oil containing 0.5% IL-AgNP as a function of the sliding distance. The addition of IL-AgNP reduced the friction by >20% and wear by ~90%. Since there was little silver, sulfur or nitrogen detected on the worn surface, the friction and wear reductions may be attributed to physical adsorption of the IL-AgNP onto the contact surface rather than chemical reactions during contact and sliding.

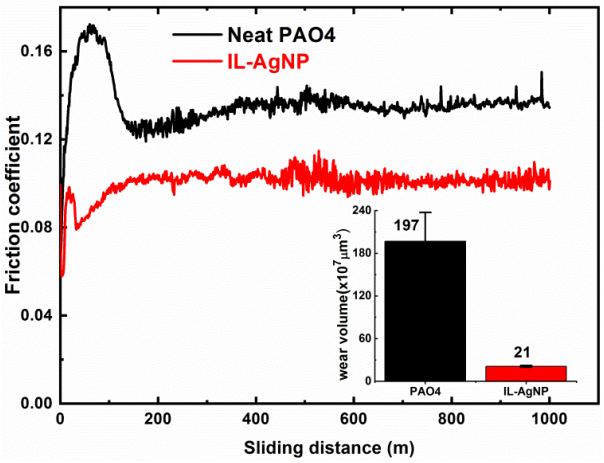

Figure 16. Comparison of the friction and wear results of a neat PAO base oil and PAO+0.50 wt% IL-AgNP.

3. Simulation Study of Friction and Wear Reduction by Addition of Functionalized NPs

During this project, the University of California Merced (UCM) team complemented experimental efforts at UTK and ORNL with multi-scale simulations of NPs and their effect on friction and wear. Our contributions can be grouped into four general areas: (3.1) development of physically realistic models of functionalized NPs, (3.2) development of atomistic models of boundary lubrication, (3.3) exploration of the effect of surface roughness and NP size using atomistic simulations, and (3.4) investigation of larger-scale NP phenomena using finite element methods. Specific contributions in each of these areas will be described in the following sections.

3.1. Develop Physically Realistic Models of Functionalized NPs

Our first goal was to develop models of the NPs being synthesized at UTK and ORNL. This includes models of hairy (polymer-functionalized) NPs, ionic liquid NPs, and thiol-functionalized NPs. First, the model hairy NPs consisted of three parts: a spherical NP, initiators and polymer chains (Figure 17). The NP was SiO_2 in β-cristobalite phase with a diameter scaled down relative

to the experimentally measured particle diameter by a factor of ten for computational efficiency. The surface of the NP was terminated by hydroxides and initiators. The number of initiators was determined from the projected area of each initiator and the diameter of the SiO_2 NP. Polymer chains where then added to a subset of the initiators on the surface. The percent coverage was determined using experimental thermogravimetric (TGA) data. Models were created of NPs with polymer chains having various lengths to study the effect of chain length on solubility. Figure 17 shows a cross-section view of a representative model of a hairy NP in 2 cSt polyalphaolefin (PAO) base oil at the end of equilibration.

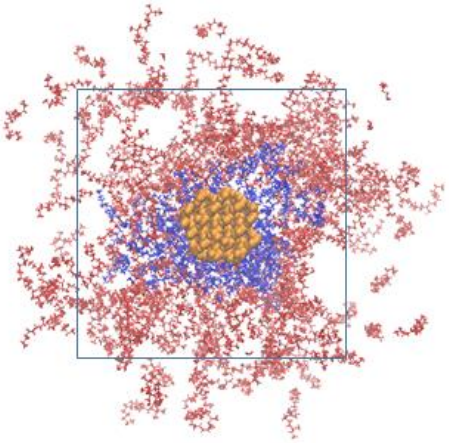

Figure 17. Cross-section view of an atomistic model of a hairy NP in PAO (yellow – SiO_2, blue – polymer, red – PAO).

Solubility is one of the main purposes of functionalizing NPs, so the models were used to understand the effect of various molecular-scale features on solubility. We modeled NPs functionalized with 6, 12, 16 and 18 carbon polymers and predicted their miscibility in PAO using a previously reported simulation method.[1] It has been proposed that two substances are miscible if the absolute difference between their solubility parameters is less than 2 $MPa^{0.5}$ and immiscible otherwise.[2] The results for our polymer functionalized NPs are shown in Table 2. The results indicate that hairy NPs functionalized with 12 carbon polymers or longer will be miscible in a simple PAO. This is consistent with experimental observations.

Table 2. Simulation-predicted miscibility of hairy NPs with varying side chain lengths in PAO. Two substances with a solubility difference ($\Delta\delta$) less than 2 $MPa^{0.5}$ are expected to be miscible.

Solute	Solubility ($MPa^{0.5}$)	Solvent	Solubility ($MPa^{0.5}$)	$\Delta\delta$ ($MPa^{0.5}$)	Miscible?
Initiated NP	8.86	PAO	14.45	5.59	No
Hairy NP (PC6MA)	9.26	PAO	14.45	5.19	No
Hairy NP (PC12MA)	14.24	PAO	14.45	0.21	Yes
Hairy NP (PC16MA)	14.49	PAO	14.45	0.04	Yes
Hairy NP (PC18MA)	13.42	PAO	14.45	1.03	Yes

The simulation method described above was observed to be accurate in predicting solubility of polymers and polymer-functionalized NPs. However, extending this method to ionic liquids (ILs) introduces several challenges. Most significantly, we found these simulations to be far more

sensitive to model parameters than the polymer studies. One factor driving this sensitivity is that we are using a non-reactive (i.e. fixed charge) empirical potential to describe the interatomic interactions, following the approach that was successfully employed for the polymer functionalized NPs. However, this requires that assumptions are made regarding the nature of the cation-anion bond in an IL. Although these assumptions are reasonable in many modeling scenarios, we found that they affect the behavior of the ILs in the PAO solvent and so affect the model-predicted miscibility. Therefore, we tested the various approximations that can be made in modeling ILs with two examples: $[P_{4444}][DEHP]$ and $[P_{66614}][DEHP]$. We set up and performed simulations of these molecules in the same model PAO as used for the polymer functionalized NP simulations. We found that the simulations were best able to reproduce experimentally-measured solubility using a simple harmonic model for the cation-anion bond. We emphasize that is a significant approximation, but a more robust model would require development of a new empirical model (force field) specifically for these ionic liquids.[3]

At ORNL, NPs were synthesized that consisted of metal inner core protected by functional groups. To complement the experimental efforts, we developed models of three functionalized silver (Ag) nanoparticles: tert-butylbenzylthiol functionalized Ag nanoparticle, fluorothiophenol functionalized Ag nanoparticle, and dodecanethiol functionalized Ag nanoparticle. Each of these consisted of a icosahedral Ag shell (13 atoms) surrounded by 6 dimeric staples (-S-Ag-S-Ag-S-).[4] The functional chains mentioned above are attached to the Sulfur atoms on the dimeric staples. Figure 18 shows snapshots of the initial configurations of the three model functionalized Ag nanoparticles.

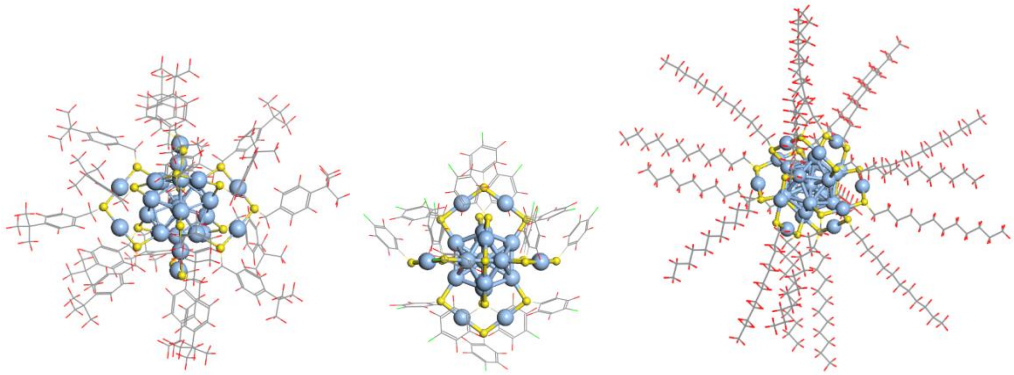

Figure 18. Models of tert-butylbenzylthiol functionalized Ag nanoparticle (left), fluorothiophenol functionalized Ag nanoparticle (center), dodecanethiol functionalized Ag nanoparticle (right).

3.2. Develop Atomistic Models of Boundary Lubrication

To understand how NPs may improve friction and wear in sliding systems, we developed novel methods of modeling boundary lubrication at the atomic scale. The premise of the modeling approach is illustrated in Figure 19. A typical tribological contact consists of multiple asperities in the interface, separated by a lubricating oil containing NPs. The atomistic model we developed captures the interface at a single asperity and the effect if individual NPs on sliding behavior.

To complement the experimental studies at ORNL on the friction behavior of functionalized nanoparticles, we modeled three functionalized NPs (see Figure 18) in boundary lubrication. We also modeled a TiO_2 particle to provide an un-functionalized reference case. In all models, the particle was placed in a simple PAO base fluid. Surface roughness was introduced as a groove perpendicular to the sliding direction on one of the surfaces. The effective roughness of the system can be varied by changing the depth of grove. The three model systems are shown in Figure 20.

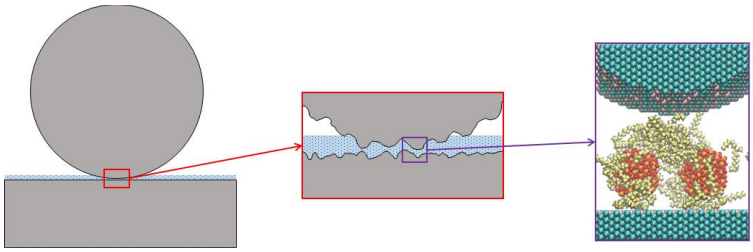

Figure 19. Theoretical premise of the approach developed to model NPs in boundary lubrication at the atomic-scale.

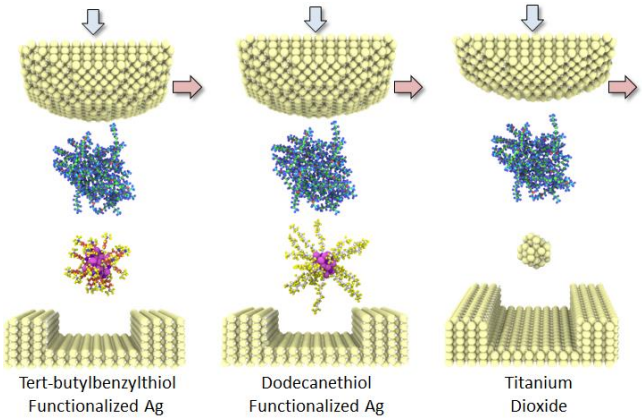

Figure 20. Snapshots of the three model systems consisting of a lower rough substrate, NP, PAO base fluid and upper asperity.

Each simulation began with the various components of the system separate from one another. Then, the asperity and substrate were brought together gradually to compress the fluid for up to 50 ns. Then, a constant normal load of 10 nN was applied and the asperity slid laterally at a constant speed of 10 m/s. Sliding continued for four cycles, where one cycle refers to atoms in the top asperity moving once across the periodic boundary in the sliding direction relative to their original positions. Friction was calculated as the lateral force resisting the motion of the top asperity. In all simulation cases, friction increased with the number of cycles due to wear during sliding. Therefore, to compare the performance of various cases, we evaluated the average friction during the fourth cycle. Wear could not be calculated using the traditional definition since the periodic boundaries did not allow atoms to be removed from the contact. However, an approximation for wear was quantified as the number of substrate atoms that were displaced through a distance of at least one lattice spacing ($\geq$ 0.5 nm). While this number is not meaningful by itself, it can be used to compare various simulation cases to one another.

The friction and wear results are shown in Figure 21. We observed no statistically significant difference between the three nanoparticles tested under these conditions. This is in contrast with experimental results which indicated that tert-butylbenzylthiol functionalized particles exhibited lower friction, but dodecanethiol functionalized particles exhibited lower wear. There are several possible reasons that the simulations did not capture this trend. The most likely reason is that our load or speed conditions were inconsistent with those in the experiment such that the lubrication regime was different. Also, there is a discrepancy in surface roughness, which we showed has a significant impact on NP effectiveness.[5] This effect was explored using multi-scale simulations, as discussed in the next two sections.

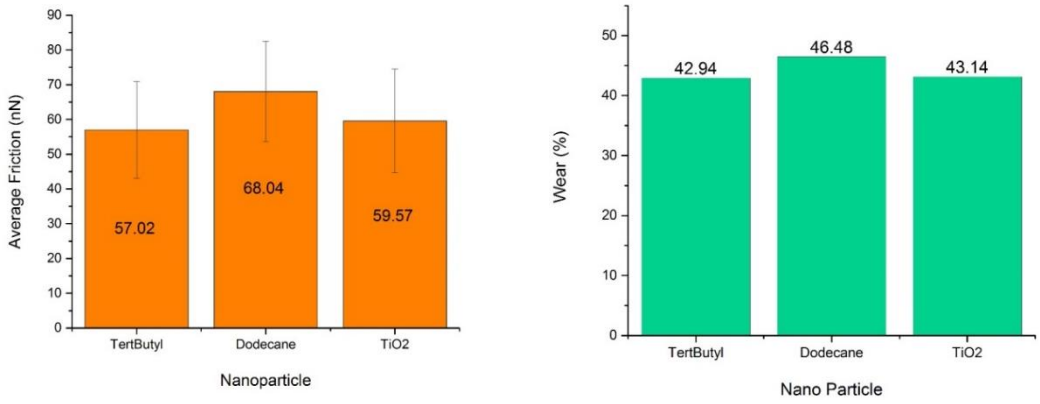

Figure 21. Comparison of the friction (left) and wear (right) for three model NPs tested at a single load and sliding speed case.

3.3. Explore the Effect of Surface Roughness and NP Size Using Atomistic Simulations

To explore the effect of surface roughness and NP size, we created models that enabled variation of those parameters. The inset to Figure 22(a) shows the friction for systems with and without the NP as functions of substrate surface roughness. We observe that, as the surface roughness increases, friction increases dramatically when only the oil present, but the NP-embedded fluid enables the friction to remain relatively constant over a range of roughness values. This result indicates that NPs may be beneficial for some surfaces and not for others. As shown in Figure 22, for a given NP size, friction may either increase or decrease, depending on the initial roughness of the surfaces. To characterize the effects of both NP size and substrate surface roughness, we ran a series of simulations at a range of sizes and roughness values. The results are summarized in the contour plot shown in Figure 22(b). Cases where adding the NP had no effect or increased friction are shown in red. The beneficial effect of the NP for all other cases is reflected by the color, where blue corresponds to the largest friction reduction. This result indicates that rougher surfaces may benefit more from the addition of NPs and that the optimum NP size can be expected to increase with substrate surface roughness.

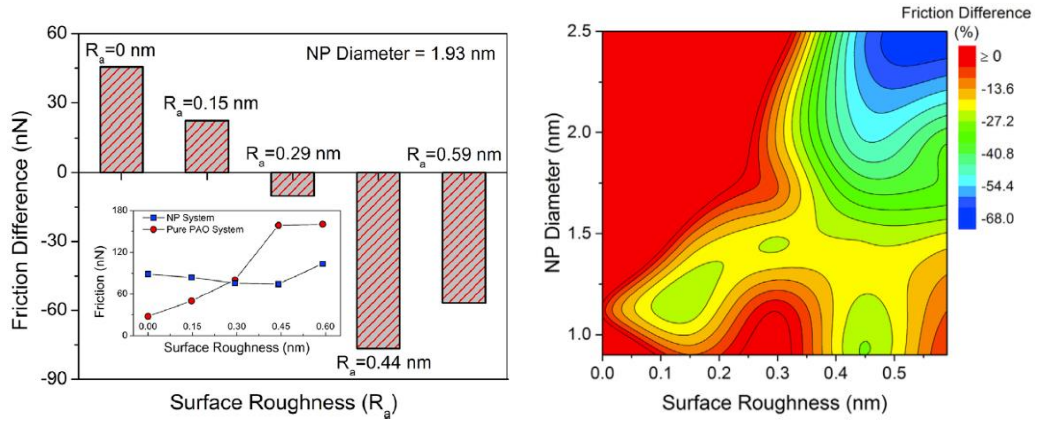

Figure 22. (a) Friction difference between the PAO2 only and the PAO2 with a 1.93 nm diameter NP systems as a function of surface roughness (simulation). Inset shows the friction with and without the NP as a function of surface roughness. (b) Contour plot of the percent difference between friction with and without an NP for a range of NP sizes and substrate roughness values.

We also used these simulations to characterize wear. Snapshots from the simulation for two cases, before and after four sliding cycles, are shown in Figure 23(a). In both of these two examples, the NP appears to mitigate surface wear. However, quantifying wear is not straightforward in the simulation since the periodic boundary conditions means that no material is removed. We therefore measured wear as the number of substrate atoms that have moved through a distance of at least one lattice spacing; while this number is not meaningful itself, but can be used to compare the various simulation cases to one another. The wear difference (percent different between cases with and without the NP) results for all NP size and substrate roughness cases are shown as a contour plot in Figure 23(b). We observe that the NP is beneficial in reducing wear in nearly all cases and that, like the friction results, NPs may be more beneficial for rougher surfaces. Overall, these findings indicates that both NP size and substrate roughness are important and, further, for a given surface roughness, an NP size can be identified that will yield minimum friction and wear.

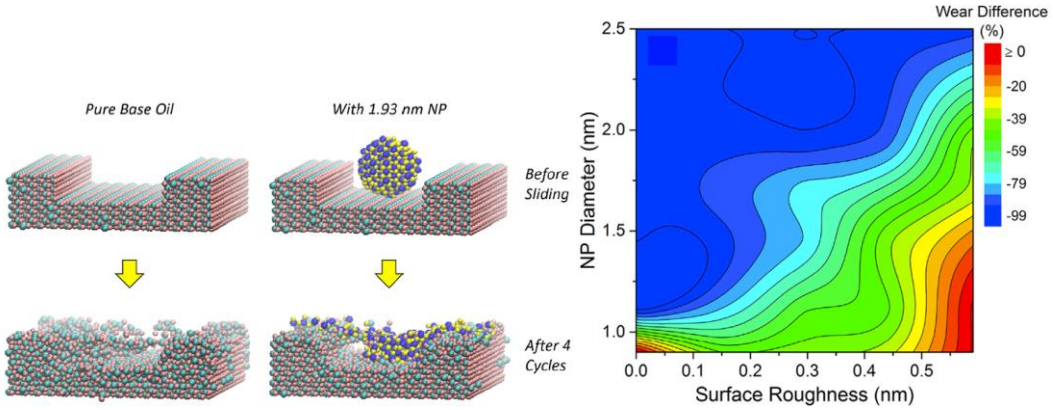

Figure 23. (a) Snapshots from the simulation for two cases illustrating the effect of the NP in mitigating surface wear. (b) Contour plot of the percent difference between wear (as quantified by surface atom displacement) with and without an NP for a range of NP sizes and substrate roughness values.

3.4. Investigate Larger-Scale NP Phenomena Using Finite Element Methods

The approach we used to capture larger-scale surface roughness was Finite Element (FE) analysis. FE simulations were performed using two-dimensional plane stain models and the Dynamic/Explicit method. We modeled sliver NPs and steel sliding surfaces. For both the NPs and surfaces, the material properties, including density, Young Modulus, Poison's ratio and stress-strain curves in the plastic region, were assumed to be those of bulk steel and silver. To investigate the effects of NP size and surface roughness, three simulations were performed where the particle diameter (D) to average surface roughness (Ra) ratio was 0.5, 1.0 or 2.0. The NP diameters were 14.4, 28.9 and 57.7 nm, and the Ra was 28.9 nm. To model the interaction between materials, the friction coefficient was chosen to be 0.2 for contact between the upper and lower steel surfaces, and 0.1 for contact between the NPs and steel surfaces. Note that the liquid lubricant is not explicitly captured in this model, so its effect is incorporated implicitly through the lower friction coefficient. The simulations were performed at pressures of 0.5 and 2.2 GPa. Figure 24 illustrates the initial configuration of the system, along with the boundary conditions, and directions of applied pressure and shear. First, load is applied, as shown in the left image, and then sliding begins, as shown in the right figure. The right figure also provides an example of the shear stress distributions that are calculated throughout the simulation.

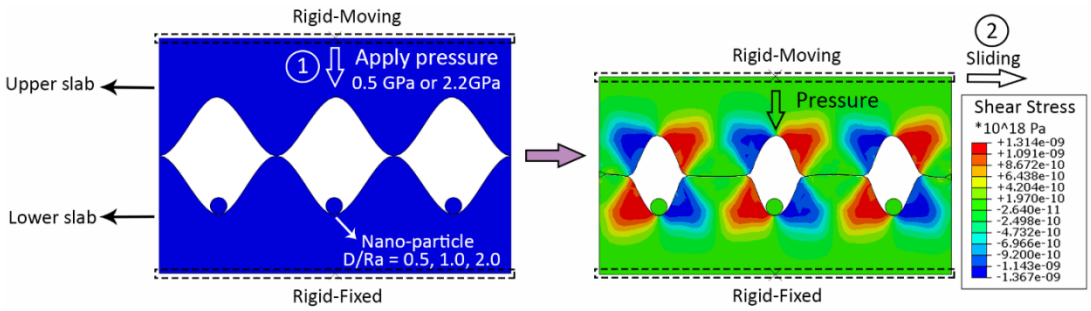

Figure 24. Initial configuration of the finite element model, where the left image shows the geometry and loading process while the right figure shows the shear stress distribution after loading at the onset of sliding.

We calculated the force in the shear direction on the upper steel surface during the first 5 seconds of the simulation and observed that there is an initial assistive force as the top asperities move from directly above and in contact with the asperities on the lower surface into the valleys on the lower surface. Then, there is a larger resistive force as the top asperities again come into contact with those of the lower surface. Friction is due to this second stage of the process. At 0.5 GPa, there are times during the process when the biggest NP yields lower friction and times when the biggest NP yields lower friction. An overall average of the force data at 0.5 GPa indicates that all NPs yield improve behavior (compared to no NP), but there is little effect of NP size. However, for the 2.0 GPa case, the two smaller NPs resulted in lower friction overall than the biggest NP. This indicates that the effect of NP size may also be sensitive to applied pressure.

We next investigated the mechanisms by which the NPs affected friction by analyzing the shear stress distributions and material deformation. Figure 25 shows snapshots of the contact between asperities on the upper and lower surface with a NP in the valley on the lower surface; images are shown at the start (left) and end (right) of contact with the NP. We observe that the harder steel asperities significantly deform the softer silver NP, which may be the early stages of the formation of a tribofilm.

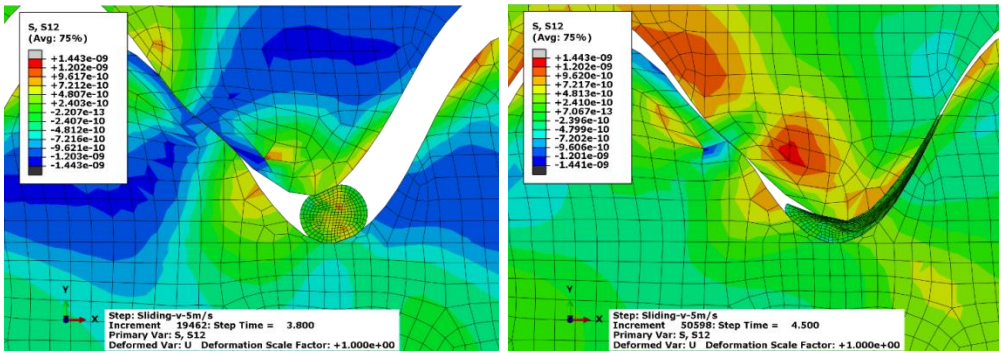

Figure 25. Snapshots of the asperities and NP at 0.5 GPa pressure in the beginning of contact (left figures) and at the end of sliding (right figures) for D/Ra=1.0.

To apply these simulations to model material wear, we implemented a recently developed technique of modeling wear in FE analysis.[6] This is a significant extension from traditional methods which only allow calculation of deformation and stress, i.e. are not able to capture

material removal. However, based on the observations from ORNL that nanoparticle size and surface roughness have a significant effect on wear, the new approach is necessary to complement those experiments with FE wear models. In this method, whether or not a deformed element is removed from the model is determined based on its plastic deformation, compressive pressure, and strain rate. The criterion for element removal is based on the Johnson-Cook damage model.[7] In our current studies, a plastic displacement limit is defined which an element must meet, in additional to the Johnson-Cook criterion, before it is removed. This approach is now being applied to model NPs in a rough contact, with realistic surface roughness and NP sizes.

References:

1. Henz, B. J.; Chung, P. W.; Andzelm, J. W.; Chantawansri, T. L.; Lenhart, J. L.; Beyer, F. L. Determination of Binding Energy and Solubility Parameters for Functionalized Gold Nanoparticles by Molecular Dynamics Simulation. *Langmuir* **2011**, *27*, 7836–7842.
2. Gupta, J.; Nunes, C.; Vyas, S.; Jonnalagadda, S. Prediction of Solubility Parameters and Miscibility of Pharmaceutical Compounds by Molecular Dynamics Simulations, *J Phys Chem B* **2012**, *115*, 2014–2023.
3. Maginn, E. J. Molecular simulation of ionic liquids: current status and future opportunities. *J. Phys.: Condens. Matter* **2009**, *21*, 373101.
4. Desireddy, A.; Conn, B. E.; Guo, J.; Yoon, B., Barnett, R. N.; Monahan, B. M.; Kirschbaum, K.; Griffith, W. P.; Whetten, R. L.; Landman, U.; Bigioni, T. P. Ultrastable silver nanoparticles. *Nature* **2013**, *501*, 399-402.
5. Peña Parás, L.; Gao, H.; Maldonado Cortés, D.; Vellore, A.; Garcia, P.; Montemayors, O.; Navam, K.; Martini, A. Effects of substrate surface roughness and nano/micro particle additive size on friction and wear in lubricated sliding. *Tribology International* **2018**, *119*, 88-98.
6. Woldman, M.; Van Der Heide, E.; Tinga, T.; Masen, M. A. A Finite Element Approach to Modeling Abrasive Wear Modes. *Tribology Transactions* **2017**, *60*, 711-718.
7. Johnson, G. R.; Cook, W. H. Fracture characteristics of three metals subjected to various strains, strain rates, temperatures and pressures. *Engineering Fracture Mechanics* **1985**, *21*, 31-48.

Peer-Reviewed Journal Publications from DE-EE0006925

1. Wright, R. A. E.; Wang, K. W.; Qu, J.; Zhao, B. "Oil-Soluble Polymer Brush-Grafted Nanoparticles as Effective Lubricant Additives for Friction and Wear Reduction", *Angew. Chem. Int. Ed.* **2016**, *55*, 8656-8660.
2. Seymour, B. T.; Wright, R. A. E.; Parrott, A. C.; Gao, H. Y.; Martini, A.; Qu, J.; Dai, S.; Zhao, B. "Poly(alkyl methacrylate) Brush-Grafted Silica Nanoparticles as Oil Lubricant Additives: Effects of Alkyl Pendant Groups on Oil Dispersibility, Stability, and Lubrication Property", *ACS Appl. Mater. Interfaces*, **2017**, *9*, 25038–25048.
3. Fu, W. X.; Bai, W.; Jiang, S. S.; Seymour, B. T.; Zhao, B. "UCST-Type Thermoresponsive Polymers in Synthetic Lubricating Oil Polyalphaolefin (PAO)", *Macromolecules* **2018**, *51*, 1674–1680.
4. Seymour, B. T.; Fu, W. X.; Wright, R. A. E.; Qu, J.; Dai, S.; Zhao, B. "Improved Lubricating Performance by Combining Oil-Soluble Hairy Silica Nanoparticles and an Ionic Liquid as an Additive for a Synthetic Base Oil", *ACS Appl. Mater. Interfaces* **2018**, revised manuscript under review.

5. Kumara, C.; Luo, H.; Leonard, D. N.; Meyer, H. M.; Qu, J. "Organic-modified silver nanoparticles as lubricant additives", *ACS Appl. Mater. & Interfaces* **2017**, *9*, 37227–37237.
6. Peña Parás, L.; Gao, H.; Maldonado Cortés, D.; Vellore, A.; Garcia, P.; Montemayors, O.; Navam, K.; Martini, A. "Effects of Substrate Surface Roughness and Nano/Micro Particle Additive Size on Friction and Wear in Lubricated Sliding" *Tribology International* **2018**, *119*, 88-98.

Presentations in Professional Conferences

1. Zhao, B. "Hybrid Ionic-Nano-Additives for Engine Lubrication to Improve Fuel Efficiency", DOE Annual Merit Review and Peer Evaluation Meeting in Washington, DC, June 6-10, 2016.
2. Zhao, B. "Hairy Nanoparticles", UT/VT workshop at University of Tennessee Knoxville Four Points Sheraton on April 18, 2016.
3. Zhao, B. "Oil-Soluble Hairy Nanoparticles as Lubricant Additives", 2016 Southeast Regional Meeting of ACS (SERMACS), October 23-26 in Columbia, SC.
4. Kumara, C. K.; Luo, H.; Leonard, D.; Meyer, H.; Qu, J. "Surface-Modified Silver Nanoparticles as Lubricant Additives", *STLE 72nd Annual Meeting*, Atlanta, GA, May 21-25, 2017.
5. Vellore, A.; Kumara, C. K.; Qu, J.; Martini, A. "Atomistic Modeling and Experimental Study of Functionalized Silver Nanoparticles as Lubricant Additives", *STLE 72nd Annual Meeting*, Atlanta, GA, May 21-25, 2017.
6. Kumara, C.; Leonard, D.; Meyer, H.; Luo, H.; Qu, J. "Organic-Modified Palladium and Silver Nanoparticles as Oil additives for Friction and Wear Reduction", *STLE 73nd Annual Meeting*, Minneapolis, MN, May 20-24, 2018.(accepted)
7. Martini, A. "Effect of Nanoparticle Size on the Tribological Properties of Nanolubricants", STLE Annual Meeting, Las Vegas NV (May 2016)
8. Gao, H. "Modeling the Effects of Nanoparticle Size and Surface Roughness on Friction in Boundary Lubrication", STLE Annual Meeting, Las Vegas NV (May 2016)
9. Zhao, B. "Hairy Nanoparticles for Lubrication", Abstract submitted for 2018 Fall ACS National Meeting in Boston, MA on August 19-23, 2018.

Invention Disclosure

1. Qu, J.; Kumara, C. "Nanoparticles as Lubricant Additives," Invention Disclosure 201704018, DOE S-138,682, Nov. 13, 2017.